

# Comparison of cumulus parameterizations and entrainment using domain-mean wind divergence in a regional model

Brian E. Mapes<sup>1</sup>, Thomas T. Warner<sup>2,3</sup>, Mei Xu<sup>2,3</sup>, David J. Gochis<sup>3,4</sup>

<sup>1</sup>*NOAA/CIRES Climate Diagnostics Center*

<sup>2</sup>*Program in Atmospheric and Oceanic Sciences,  
University of Colorado, Boulder*

<sup>3</sup>*Research Applications Program,  
National Center for Atmospheric Research*

<sup>4</sup>*Advanced Study Program,  
National Center for Atmospheric Research*

Corresponding author address:

Brian Mapes, CIRES, Box 216 UCB, Boulder, CO 80309-0216, USA      email: brian.mapes@noaa.gov

*J. Amos. Sci.*

Submitted August 2002, Revised May 2003 and Oct 2003

## ABSTRACT

Several different cumulus parameterizations are compared in a 10-day regional model simulation over the tropical Americas in northern summer. A simple bulk diagnostic test is devised, comparing the model's preferred domain-mean wind divergence profile with 'observed' divergence. The latter is obtained by a line integral of the normal wind component at the model's outer boundary, from the ECMWF reanalysis data used as lateral boundary conditions. The former is obtained from a line integral one gridpoint in from the boundary, a perimeter which encloses almost exactly the same region. Even though the model fields near the boundary are strongly nudged toward the ECMWF values, the difference is distinct, and indicative of systematic errors in the model's heating field throughout the interior of the domain. Heating reflects the effects of the convection scheme, both directly and indirectly (e.g. through its impact on resolved condensation). A useful axis along which to characterize schemes appears to be overactive vs. underactive. Underactive convective schemes tend to produce too little low-level convergence and upper-level divergence, while overactive schemes produce too much. This categorization is also reflected in rainfall fields, as overactive schemes produce widespread light convective rain while underactive schemes produce sparse occasional storms. For example, the Kain-Fritsch scheme is overactive with its default entraining-plume radius of 1500m, a value optimized for midlatitudes over land. A value of 750m makes the regional divergence magnitude about right, but makes the upper-tropospheric outflow altitude too low, illustrating a classic dilemma of entraining-plume models of convection. Schemes with other conceptual structures give widely varying divergence errors. The largest errors are found with the Anthes-Kuo scheme, while the smallest errors are found with the Betts-Miller-Janjic scheme, which has no consistent divergence bias over time. Diagnosis of other North American monsoon simulations supports the general underactive/overactive characterization, but shows that the best scheme and parameters may depend on weather regime.

# 1 Introduction

Many different cumulus parameterization schemes are available for regional and global atmosphere models that do not resolve convective clouds explicitly. Different schemes have different design histories, and in some cases completely different conceptual underpinnings. In the community regional model known as MM5, users choose from among 7 options, with the main formal guidance in the documentation (Grell et al. 1994) consisting of suggested ranges of horizontal resolution, as envisioned by the designers of the schemes. Convection scheme intercomparisons have been published, in both short-term forecast mode (Wang and Seaman 1997, Yang et al. 2000) and longer forced runs (Gochis et al. 2002). Results are difficult to summarize or generalize, since they depend on different measures of performance, and may be specific to the region, season, weather type, resolution, forecast range, etc. This ambiguity is unavoidable to some extent, and users may always want to optimize the model with multidimensional measures specific to their applications. Still, it seems desirable to have a simple, objective, low-dimensional diagnosis of some relevant, systematic aspects of performance. This article reports an attempt to develop such a diagnosis, reflecting diabatic model physics, with convection as a special focus. Our particular application is regional climate simulations over South and Central America, with the objective of a general scientific understanding of rainfall-generating weather processes. For present purposes, then, ‘relevant’ and ‘systematic’ aspects of performance refer to space and time averages of rainfall and heating, with no focus on a special forecast location or time.

There are several properties that we would like such a diagnosis to possess. The first desirable property, almost too obvious to mention, is that a diagnosis should be sensitive to the aspects of model configuration one hopes to optimize and study: in this case convection schemes and their parameters. Second, a diagnosis should have appropriate dimensionality, in terms of both the

number and character of retained dimensions. But what is appropriate?

The model's full suite of space-time fields seems clearly too high-dimensional for systematic intercomparison and evaluation. While much can be gleaned from intimate inspection of the internal details of many fields at many times, it is very time-consuming, and results are ultimately subjective and hard to share or generalize. Even a time sequence of rainfall maps is almost too much data to evaluate cleanly. At the other extreme, a single scalar like domain-averaged accumulated precipitation is too uninformative. It would be better to keep, say, the time dimension, even though we have no special interest in a particular time, in order to gain the self-evident statistical significance that comes when the viewer can divide the diagnosis into arbitrary subsets by eye. Ultimately, results must be published in two-dimensional diagrams. Since we have no special interest in a particular location, the horizontal dimensions seem to be good candidates for collapsing out of the diagnosis, by constructing horizontal averages. The divergence diagnosis developed here is thus two-dimensional, with the height dimension (which is of special physical interest) and time, supplemented by time-longitude rainfall diagrams for weather context.

A third desirable property for a diagnosis is that it should allow comparison of the model simulations to observations, not just to other simulations. This is the essence of the scientific method, and hence important to our objectives, but has subtle difficulties in the specific case of a regional model. A global reanalysis of real weather is used as the source of initial and lateral boundary conditions for the model. Comparison of the model solutions with independent data (like satellite-derived rainfall estimates here) is one useful technique, but could merely reflect inconsistencies between the independent data sets. However, if the simulations show strong systematic inconsistency with credible, large-scale aspects of the very reanalysis data used to drive

them, this increases our confidence in attributing the mismatch to shortcomings of the regional modeling system. The joint examination of independent-data comparisons and boundary data comparisons is especially useful in linking errors to internal model physics.

Our diagnosis centers on horizontal wind divergence, for the following reasons. Through the mass continuity equation, divergence is linked to vertical motion, which in the stratified tropical troposphere is in turn indicative of heating processes. For this reason, we expect divergence to be sensitive to differences in convection schemes or their internal assumptions, as they strongly affect the field of total heating. It is important to note that total heating includes important contributions by indirect but associated effects of convection, such as nonconvective condensation and cloud-radiation interaction. While these contributions could be separated in the model, observations are insufficient to validate the separate parts. The momentum-flux properties of convection should not affect domain-averaged divergence, except perhaps through small secondary-circulation effects if convection alters balanced momentum fields at the domain perimeter.

A true horizontal domain average of divergence is easily computed, making use of the divergence theorem, by constructing the line integrals of the normal wind component around the domain perimeter. This is a useful property of divergence, since the reanalysis boundary data are only specified at the perimeter. Performing the same computation for winds one gridpoint in from the boundary yields an average over almost the same horizontal area. The technique is discussed further below. At the least, this approach tests the consistency of the model with its forcing data, evaluating basic assumptions underlying the regional modeling exercise. To the extent that regional-scale average divergence is depicted realistically in global reanalyses, comparison with reanalysis may constitute a true comparison of model against nature, allowing one to state that

some scheme or parameter value is actually better or worse than another. It is hoped that this limited but objective diagnosis of the complex relationship between local assumptions inside convection schemes and their highly averaged performance in this particular model can highlight opportunities for improvement of convective closure assumptions more generally.

## **2 Model and simulation details**

Our simulations are centered on northwestern South America in northern summer (28 August to 7 September, 1998). The Pennsylvania State University / National Center for Atmospheric Research mesoscale model MM5 version 3 was used, with Dudhia simple ice microphysics and radiation options (Grell et al. 1994). This paper reports tests of several convection schemes, which are already implemented in the modeling system and are simply selected by the user with a switch in the code. More details of the model are mentioned below as needed, and the project and results are reported more fully in Warner et al. (2003) and Mapes et al. (2003b). Figure 1 shows the region of our largest model domain, with topography shaded and boxes indicating the locations of nested grids used in some runs. The domain of Fig. 1 was covered with a 72 km grid increment. In some nested-grid runs, the larger box within Fig. 1 had a 24 km grid increment, and the smaller box had an 8 km grid increment. Nesting was found to make almost no difference to the domain-averaged results (discussed further below).

We now review the MM5 boundary-condition protocol, which is important for understanding the results here. More detailed description is in Grell et al. (1994). The values of all fields were specified on the outermost row of grid points, from a spatial and temporal interpolation of twice-daily 2.5-degree gridded European Center for Medium-range Weather Forecasting (ECMWF) global reanalysis. The twice-daily sampling (00 UTC and 12 UTC) distorts the diurnal

cycle, linearly interpolating between morning and evening over South America. One consequence of this is that the eastern domain boundary at 50W has a mid-day temperature contrast across it that acts somewhat like a land-sea contrast, generating a “boundary breeze” that artificially spawns north-south convective bands over the Amazon (see Appendix of Warner et al. 2003). In subsequent simulations reported there, the boundary was moved to 30W to avoid this artifact, but for present purposes we retained the boundary at 50W, since this regime (convection schemes interacting with gravity waves) was deemed to be of unique physical interest and a useful counterpoint to the easterly waves in the northern part of the domain (where convection interacts with rotational disturbances). Additionally, diurnally initiated squall lines do exist in nature (Garstang et al. 1994, Cohen et al. 1995), crossing South America in 2-3 days.

The first three rows of gridpoints in from the boundary have their fields relaxed toward reanalysis values with time scales of 10, 20, and 30 time steps, respectively. Inside this ‘buffer zone’ of 3 gridpoints nearest the boundaries, the model fields are solutions of its dynamical and physical equations without these extra relaxation terms.

### **3 Results**

Figure 2 shows time-longitude plots of satellite-estimated rainfall for the northern and southern halves of the domain (see Mapes et al. 2003a for details and additional contextual data). In the northern half (8N-26N, Fig. 2a), dark areas sloping up to the left indicate disturbances that traveled east to west in the western Atlantic and Caribbean, here called easterly waves. Figure 2a indicates that the modeled period contains three distinct easterly waves. Two are in the model domain at the initial time (day 240), and hence are in the model initial conditions, while the third enters through the eastern boundary conditions on days 243-244. A massing of convective activity

and rainfall is also seen west of 90W, in the eastern Pacific. In the southern half (11S-8N, Fig. 2b), diurnal variation of rainfall is more dominant over South America, with multi-day westward-moving rain features here called Amazon squall lines. In short, a diverse array of both dynamically and diurnally modulated tropical convective weather phenomena are included in the domain of these simulations.

Our control simulation used the Kain-Fritsch convection (Kain and Fritsch 1990, 1993; Kain 2003) scheme, with a 750m radius for its entraining plume, on three nested grids. Note that the default radius in the Kain-Fritsch scheme is 1500m. The control simulation is described in more detail in Warner et al. (2003). A summary diagnosis figure for the control case is shown in Fig. 3, and is a template for later figures. Panels a and c are rainfall time-longitude diagrams, which can be compared directly to Fig. 2. Total rain is shaded, while nonconvective rain is indicated by dotted contours. Panel b shows profiles of time-averaged, area-averaged wind divergence, obtained from the average of the normal wind component around closed perimeters, multiplied by the perimeter to area ratio of the region in question ( $8 \times 10^{-7} \text{ m}^{-1}$ ). For tropical scaling relevant to this situation, the wind divergence profile as measured at the perimeter is closely related to the heating profile within the domain (Mapes and Houze 1995). Since the same reanalysis data are used as boundary conditions for all runs, this solid line is the same in all subsequent figures. The other 3 lines (dotted, dashed, dash-dot) were computed from normal wind components one, two, and three grid points inside the boundary, respectively.

The three broken curves in panel b differ increasingly from the ECMWF analyzed regional wind divergence, typically in a monotonically increasing way. We interpret these differences as pointing in the direction of systematic model error, i.e. toward the divergence profile the

model would tend to generate if it were not so forcibly constrained to agree with the observational analysis. The difference between the one-gridpoint-in and ECMWF divergence is shown in time-height section in panel d. Typically, the errors develop rapidly and are consistent throughout the period of the simulation, suggesting that the time-mean differences of panel b are indicative of systematic model bias with respect to the ECMWF reanalysis.

In the control case, the rainfall simulation is reasonably close to observations in both rainfall and divergence measures, although it still has shortcomings. The easterly waves develop too readily into tropical cyclones (Fig. 3a), while the Amazon squall lines are excessively regular (Fig. 3c). The model divergence differs modestly from ECMWF (panel b), with some excesses of low-level convergence and middle-level divergence. The main divergence level in the upper troposphere is too low. These differences develop quickly and are consistent through time (panel d).

The wind divergence differences in panels b and d of Figs. 3-8 imply vertical motions in the buffer zone itself. Very large vertical advective tendencies of temperature, moisture, cloud, etc. in the buffer zone are implied by some of these results. These tendencies will tend to produce differences between model values and reanalysis boundary values, until the relaxation terms grow to balance them. Peculiar rainfall amounts in the buffer zone sometimes offer a glimpse of the strange conditions prevailing there (e.g. Fig. 6b of Gochis et al. 2002), but buffer-zone biases or relaxation tendencies in other fields are beyond the present scope.

## **4 Comparison of parameter settings and other schemes**

Figures 4 through 8 are identical in format to Fig. 3, for various settings of internal parameters in the Kain-Fritsch scheme and for some other schemes. For example, the standard Kain-Fritsch run (STDKF, with 1500m plume radius, Fig. 4) produces a better simulation of the altitude

of maximum divergence (higher), but with excessive strength (Fig. 4b). This seems consistent with changes to the rainfall field, in the sense that lower entrainment of environmental air by convective plumes allows greater lifted buoyancy, encouraging excessive widespread light precipitation, which is almost entirely convective (Fig. 4a). Table I shows the fraction of nonconvective precipitation in the northern and southern halves of the domain for various runs. In STDKF, the values are 17%, compared to almost twice that in the control run.

Nested-grid runs are computationally more complex and expensive than single-grid runs, so for ease of experimentation the largest domain (at 72 km grid increment) was run alone, without nesting in the following runs. Comparing this one-domain run to the control (Fig. 3) showed almost no detectable difference in the divergence profile diagnostics (not shown). One visually noticeable difference of all runs without nested grids, including the no-nest run with control-run parameters, is the appearance of some terrain-locked rainfall features over the poorly-resolved topography, which appear as vertical stripes in panels a and c of Figs. 5-8. These are typically from explicit condensation, not parameterized convective rainfall (e.g., compare NONEST to CONTROL in Table I in the southern half of the domain).

The NOTRIG run (Fig. 5) differed from the control only in having the trigger function (Kain and Fritsch 1992) modified. Specifically, the artificial buoyancy increment added to the entraining plume's buoyancy, based on grid-resolved vertical velocity, is set to zero. In this case the Amazon squall lines fail to propagate (Fig. 5c), as might be expected from the analysis of their mechanism in the appendix of Warner et al. (2003), but the divergence errors are even smaller than in the control run. This suggests that the excessive boundary-spawned squall-line activity, attributable to having the eastern boundary at 50W in these runs (c.f. Fig. 5 of Warner et al. 2003),

may be partly responsible for the remaining modest divergence errors in the control run. This interpretation is not completely clean, however, since other aspects of the simulation also changed. For example, the easterly-wave rainfall is also significantly affected by the modified trigger function (Fig. 5a).

Other runs tested entirely different convection schemes, also examined in Wang and Seaman (1997), Yang et al. (2000), and Gochis et al. (2002). The appendices of those papers review more details of the schemes. The KF scheme involves an entraining and detraining plume, with a trigger function based on low-level vertical velocity. The Grell (1993) scheme uses undiluted parcel buoyancy to determine cloud top, and has a closure based on the rate of destabilization by grid-scale processes. The Anthes-Kuo scheme (Anthes 1977) consults a parcel buoyancy to determine if potential buoyancy exists, then decides the amount of convection based on moisture convergence. The Betts-Miller scheme (BMJ, Betts and Miller 1986, Janjic 1994) adjusts the gridpoint profiles of temperature and moisture toward empirically-defined modified moist adiabats.

The results of the GRELL run (Fig. 6) show spotty but intense rainfall, not well organized into easterly waves or Amazon squall lines. Apparently the scheme is reluctant to activate, frequently yielding little or no rain. Where rainfall does develop, it is very intense. As mentioned by Yang et al. (2000), this scheme tends to nucleate rainstorms of explicit condensation, which at low resolution tend to be intense and spotty (dotted contours in panels a,c). Table I indicates that, with this scheme, 60-70% of the rainfall comes from large-scale condensation. The divergence test concurs with these considerations, in that this 1993 version of the Grell convection scheme also produces a too-weak area-averaged divergence profile (Fig. 6b). However, the altitude of the

upper-tropospheric divergence is higher, and in better agreement with reanalysis. This success is apparently attributable to the scheme's use of an undiluted (non-entraining) plume to determine its convective top height. The alternative closure prevents the scheme from suffering the associated shortcoming of a low entrainment rate: overactivity, as seen in the STDKF experiment.

The Anthes-Kuo scheme (Fig. 7) also produces weak and poorly organized rainfall patterns, and almost no area-averaged low-level convergence: only the most strongly nudged row of gridpoints, one in from the boundary, has a convergent mean normal wind below 650 hPa! In this simulation, the MM5 tries to produce a strong regional upward motion in the upper half of the troposphere, highly inconsistent with the ECMWF boundary conditions. These results are so far from realistic that we have not explored them in much detail. While the scheme is underactive, explicit condensation is also small in this run (12-15% in Table I). In fact, it is easily seen by eye that the total rainfall in this run is extremely low compared to the other runs.

The BMJ run (Fig. 8) produced smooth propagating streaks in the rainfall field, whose texture and dynamic range are generally fairly comparable to the satellite observational estimates. In the southern half of the domain, the scheme is less successful. It has the smallest domain-average divergence errors of any of the schemes tested: at no altitude is the error consistent in sign throughout the 10-day simulation period (Fig. 8d). Although it does not refer to mass flux or entrainment explicitly, the carefully defined empirical moist adiabat used by this scheme apparently contains accurate information about the vertical structure of convective processes. With the BMJ scheme, explicit condensation accounts for only 4-5% of the total rainfall.

To give a wider perspective on some of the results, similar diagnosis was undertaken of a different context, namely the North American summer monsoon simulations of Gochis et al.

(2002, hereafter GSY), which used the U.S. National Centers for Environmental Prediction (NCEP) reanalysis for boundary conditions. Figure 9 presents divergence profiles equivalent to panel d of Figs. 3-8 for simulations with the standard KF, Grell, and BMJ schemes used on an inner grid with 30 km resolution, nested within a larger domain at 90 km resolution which used the BMJ scheme in all runs. The figure shows a sensitivity to the inner-grid convection scheme in the late summer when convection is active, but much less in the early summer (not shown).

The KF scheme yields only small divergence errors, while the Grell and BMJ schemes are underactive in this case, producing too-weak domain-averaged divergence compared to that implied by the reanalysis. GSY showed more directly that these schemes were underactive: they yielded too little rainfall, and produced a more convectively unstable time-mean state. Consistent with the latter, in light of the mechanisms described by Warner and Hsu (2000), GSY found an unrealistic intense band of rainfall right at the upwind boundary where unstable air from the coarse-grid domain enters the finer-grid domain with the KF scheme (their Fig. 6b). In their simulations, the KF scheme performed well with the standard plume radius of 1500m, which may indicate that this value is appropriate to the deeper boundary layers characteristic of the semiarid regions of convection in GSY's domain. The underactivity of the BMJ scheme in GSY's simulations, in contrast to our results in Fig. 8, may also reflect differences between semiarid-monsoon and oceanic-tropical convection. On the other hand, these differences could somehow reflect different biases, between the ECMWF and NCEP reanalyses, or between these two distinct regions. In any case, the divergence test appears to be a useful, low-dimensional diagnosis of at least relative convection scheme performance in more than one simulation context.

## 5 Conclusions

The domain-averaged divergence has been shown to be sensitive to convection schemes, and to values of the entrainment parameter within a given scheme. Diagnosis of the divergent wind near the model boundary is indicative of heating processes throughout the model domain, at least in equatorial and tropical latitudes where the domain is not much larger than a Rossby deformation radius. The results are conveniently one-dimensional (in the vertical), with optional resolution in time to indicate their robustness. Each simulation is directly compared against what we presently, for convenience, will call observations (ERA-15 reanalysis). This technique attempts to make positive use of an untidy aspect of regional modeling which can otherwise be more of a hindrance to diagnosis and interpretation: the imposition of lateral boundary conditions (Warner et al. 1997, Marbaix et al. 2003). The confrontation of model and observations occurs in a reasonable physical regime, since the boundary nudging terms act to keep the basic state fairly realistic.

One nagging question is whether global reanalysis fields really have the status of ‘observations’, against which regional model fields should be judged. Reanalysis data have biases which reflect the physical parameterizations of the reanalysis model, a problem which may be particularly severe with regard to structure in the vertical dimension where the dynamical constraints used in data assimilation are not as tight. On the other hand, the quantity consulted in this diagnosis is wind divergence on a quite large scale, 60 degrees longitude by 35 degrees latitude, so it may be reasonable to hope that reanalyses would be fairly well constrained by observations at this scale (Newman et al. 2000). Also, temporal interpolation between morning and evening reanalyses certainly distorts and underestimates the diurnal cycle one would expect in the region of a large continent. Diurnal variations of ECMWF-MM5 differences are clearly present in Figs. 4d and 7d, but we would not necessarily interpret them as model errors.

The divergence test here agrees with rainfall fields about underactive/overactive characterization, but also offers vertical structure information. For example, we can see fresh objective evidence of an old dilemma of entraining plumes. A larger entrainment rate, while useful for restraining a convection scheme from raining too easily, does so at the cost of accuracy in other properties -- in this case, the altitude of upper-level outflow (c.f. Warner 1970, Reuter 1986, Emanuel and Zivkovic-Rothko 1999). These considerations also seem to hold for global models, in which convection schemes with too little entrainment in the plumes used for convection-scheme closure tend to rain too easily, producing bland widespread tropical rainfall fields with too little variability in both space and time (Tokioka et al 1989, Ose et al 1989, Kiehl et al. 1999, Lee et al. 2003). However, too-large entrainment rates tend to excessively limit the top height of convection, contributing to the problem of upper-tropospheric cold biases (Milton et al. 2002).

For the Kain-Fritsch scheme, entrainment is a major adjustable parameter for tuning the scheme. It is physically satisfying that the value of 750m for entraining-plume radius, which we found here to minimize divergence error and some related rainfall bias problems, is closer to the boundary-layer depths in the moist tropics than is the default value of 1500m, derived for continental storms where the subcloud layer is deeper. Perhaps a boundary layer depth-dependent radius could work in a wider range of situations. Larger adjustments or redesigns of entraining plume calculations might also be helpful (Kain 2003).

In this work, the Betts-Miller scheme (Betts and Miller 1986, Janjic 1994) performs better than more physically-elaborated schemes with many more lines of code. Apparently there is powerful truth to the scheme's basic assumption that convection tends to adjust the atmosphere toward a modified moist adiabat. The scheme's empirical encapsulation of the structure of that moist adi-

abat also apparently contains good information on the vertical structure of convection, as this scheme had the lowest systematic divergence errors of any tested. Despite its impressive success, this scheme cannot replace schemes based on mass flux for many applications, since the latter can interface more satisfyingly with other fields and processes such as cloudiness and tracer transport. The other schemes tested here, with closures based on derivatives of state variables (moisture convergence rate or destabilization rate), were both underactive. The Anthes-Kuo scheme in particular performed very poorly. The Kain-Fristch scheme performed the best in the simulations considered here, and became our control run, but it exhibits the too-low outflow problem commonly encountered with entraining plumes.

## **Acknowledgements**

This research was supported by the U.S. NOAA Office of Global Programs, under the Pan-American Climate Studies (PACS) program, grant number NA96GP0051. The initial manuscript was much improved by anonymous reviews, and by comments from Jack Kain and Peter Bechtold.

## References

- Anthes, R. A., 1977: A cumulus parameterization scheme utilizing a one-dimensional cloud model. *Mon. Wea. Rev.*, **105**, 270-286.
- Betts, A.K., and M.J. Miller, 1986: A new convective adjustment scheme. Part I: Observational and theoretical basis. *Quart. J. Roy. Meteor. Soc.*, **112**, 677-692.
- Cohen, J., M. Silva Dias, and C. Nobre, 1995: Environmental conditions associated with Amazon squall lines: A case study. *Mon. Wea. Rev.*, **123**, 3163-3174.
- Emanuel, K.A., and M. Zivkovi-Rothman, 1999: Development and evaluation of a convection scheme for use in climate models. *J. Atm. Sci.*, **56**, 1766-1782.
- Garstang, M., H.L. Massie, Jr., J. Halverson, S. Greco, and J. Scala, 1994: Amazon coastal squall lines. Part I: Structure and kinematics. *Mon. Wea. Rev.*, **122**, 608-622.
- Gochis, D. J., W. J. Shuttleworth, and Z.-L. Yang, 2003: Sensitivity of the modeled North American Monsoon regional climate to convective parameterization. *Mon. Wea. Rev.*, **130**, 1282-1298.
- Grell, G. A., 1993: Prognostic evaluation of assumptions used by cumulus parameterizations. *Mon. Wea. Rev.*, **121**, 764-787.
- Grell, G. A., J. Dudhia, and D. R. Stauffer, 1994: *A description of the fifth generation Penn State/NCAR mesoscale model (MM5)*. NCAR Technical Note, NCAR/TN 398+STR, 138pp.
- Janjic, Z.I., 1994: The step-mountain eta coordinate model: further developments of the

convection, viscous sublayer and turbulence closure schemes. *Mon. Wea. Rev.*, **122**, 927-945.

Kain J. S. and J. M. Fritsch, 1990: A one-dimensional entraining/detraining plume model and its application in convective parameterization. *J. Atmos. Sci.*, **47**, 2784-2802.

Kain, J. S., and J. M. Fritsch, 1992: The role of the convective “trigger function” in numerical forecasts of mesoscale convective systems. *Meteor. Atmos. Phys.*, **49**, 93-106.

Kain J. S. and J. M. Fritsch, 1993: Convective parameterization for mesoscale models: The Kain-Fritsch scheme. *The Representation of Cumulus Convection in Numerical Models*. Meteor. Monogr., No. 46, Amer. Meteor. Soc., 165-170.

Kain, J. S., 2003: The Kain-Fritsch convective parameterization: an update. *J. App. Meteor.*, conditionally accepted.

Lee, M.-I., I.-S. Kang, and B. E. Mapes, 2003: Impacts of cumulus convection parameterization on aqua-planet simulations of tropical intraseasonal variability. *J. Meteor. Soc. Japan*, in press.

Mapes, B.E., and R.A. Houze, Jr., 1995: Diabatic divergence profiles in west Pacific mesoscale convective systems. *J. Atmos. Sci.*, **52**, 1807-1828.

Mapes, B.E., T.T. Warner, and M. Xu, 2003a: Diurnal patterns of rainfall in northwestern South America. Part I: Background and context. *Mon. Wea. Rev.*, **131**, 799-812.

Mapes, B.E., T.T. Warner, and M. Xu, 2003b: Diurnal patterns of rainfall in northwestern South America. Part III: Diurnal gravity waves and night-morning offshore convection. *Mon.*

*Wea. Rev.*, **131**, 830-844.

Marbaix, P., H. Gallée, O. Brasseur, and J.-P. van Ypersele. 2003: Lateral boundary conditions in regional climate models: A detailed study of the relaxation procedure. *Mon. Wea. Rev.*, **131**, 461-479.

Newman, M., P.D. Sardeshmukh, and J. W. Bergman, 2000: An assessment of the NCEP, NASA, and ECMWF reanalyses over the tropical west Pacific warm pool. *Bull. Amer. Meteor. Soc.*, **81**, 41-48.

Ose, T., T. Tokioka, and K. Yamazaki, 1988: Hadley circulations and penetrative cumulus convection. *J. Meteor. Soc. Japan*, **67**, 605-619.

Reuter, G. W., 1986: A historical review of cumulus entrainment studies. *Bull. Amer. Meteor. Soc.*, **67**, 151-154.

Tokioka, T., K. Yamazaki, A. Kitoh, and T. Ose, 1989: The equatorial 30-60 day oscillation and the Arakawa-Schubert penetrative cumulus parameterization. *J. Meteor. Soc. Japan*, **66**, 883-901.

Wang, W., and N. L. Seaman, 1997: A comparison study of convective parameterization schemes in a mesoscale model. *Mon. Wea. Rev.*, **125**, 252-278.

Warner, J., 1970: On the steady-state one-dimensional models of cumulus convection. *J. Atmos. Sci.*, **27**, 1035-1040.

Warner, T.T., R.A. Peterson, and R.E. Treadon, 1997: A tutorial on lateral boundary condi-

tions as a basic and potentially serious limitation to regional numerical weather prediction. *Bull. Amer. Met. Soc.*, **78**, 2599-2617.

Warner, T. T., and H.-M. Hsu, 2000: Nested-model simulations of moist convection: the importance of coarse-grid parameterized convection on fine-grid resolved convection. *Mon. Wea. Rev.*, **128**, 2211-2231.

Warner, T. T., B. E. Mapes, and M. Xu, 2003: Diurnal patterns of rainfall in northwestern South America. Part II: Model simulation and comparison with observations. *Mon. Wea. Rev.*, **131**, 813-829.

Yang, M.-J., F.-C. Chen, and M.-D. Cheng, 2000: Precipitation parameterization in a simulated Mei-Yu front. *J. Terrestrial, Atmos. and Oceanic Sci. (TAO)*, **11**, 393-422.

**Table 1: Nonconvective rain fraction (%) in the northern and southern halves of the domain of the various simulations discussed in the text.**

|         | CONTROL | NONEST | STDKF | NOTRIG | GRELL | KUO | BMJ |
|---------|---------|--------|-------|--------|-------|-----|-----|
| N. half | 32      | 32     | 17    | 36     | 60    | 12  | 4   |
| S. half | 26      | 34     | 17    | 47     | 71    | 15  | 5   |

## Figure captions

Figure 1: Base map of the region covered by this modeling study. Boxes indicate the nested model grids (see Part II for details), and topography is indicated with shading at the resolution of the model (filled contours, 200m contour interval).

Figure 2: Time-longitude plots of an observational rainfall estimate (the GPI precipitation index, equal to  $3 \text{ mm h}^{-1}$  times the fractional coverage of infrared brightness temperatures  $< 235\text{K}$ ) for the 10-day period of the simulations. a) Northern half of the domain, 8-26N. b) Southern half, 11S-8N.

Figure 3: Summary of simulation results, for the control case (nested grids, Kain-Fritsch scheme, 750m plume radius, with trigger function). Left panels (a,c): model rainfall time-longitude sections, comparable to Fig. 2. Shading is total rainfall, dotted contours indicate nonconvective rainfall, interval 0.2 mm/h. b) Time mean divergence profiles, obtained by normal wind component line integrals 0 (solid), 1 (dotted), 2(dashed), 3 (dot-dashed) gridpoints in from the boundary. d) time-height section of the difference between divergence obtained from line integrals 1 and 0 gridpoints in from the boundary.

Figure 4: As in Fig. 3, but for standard Kain-Fritsch settings (1500m entraining plume radius).

Figure 5: As in Fig. 3, but with the trigger function disabled.

Figure 6: As in Fig. 3, but for the GRELL scheme.

Figure 7: As in Fig. 3, but for the KUO scheme.

Figure 8: As in Fig. 3, but for the BMJ scheme.

Figure 9: As in fig. 3d, but for the North American summer monsoon simulations of Gochis and Shuttleworth (2003), averaged over 15 July to 2 August, 1999.

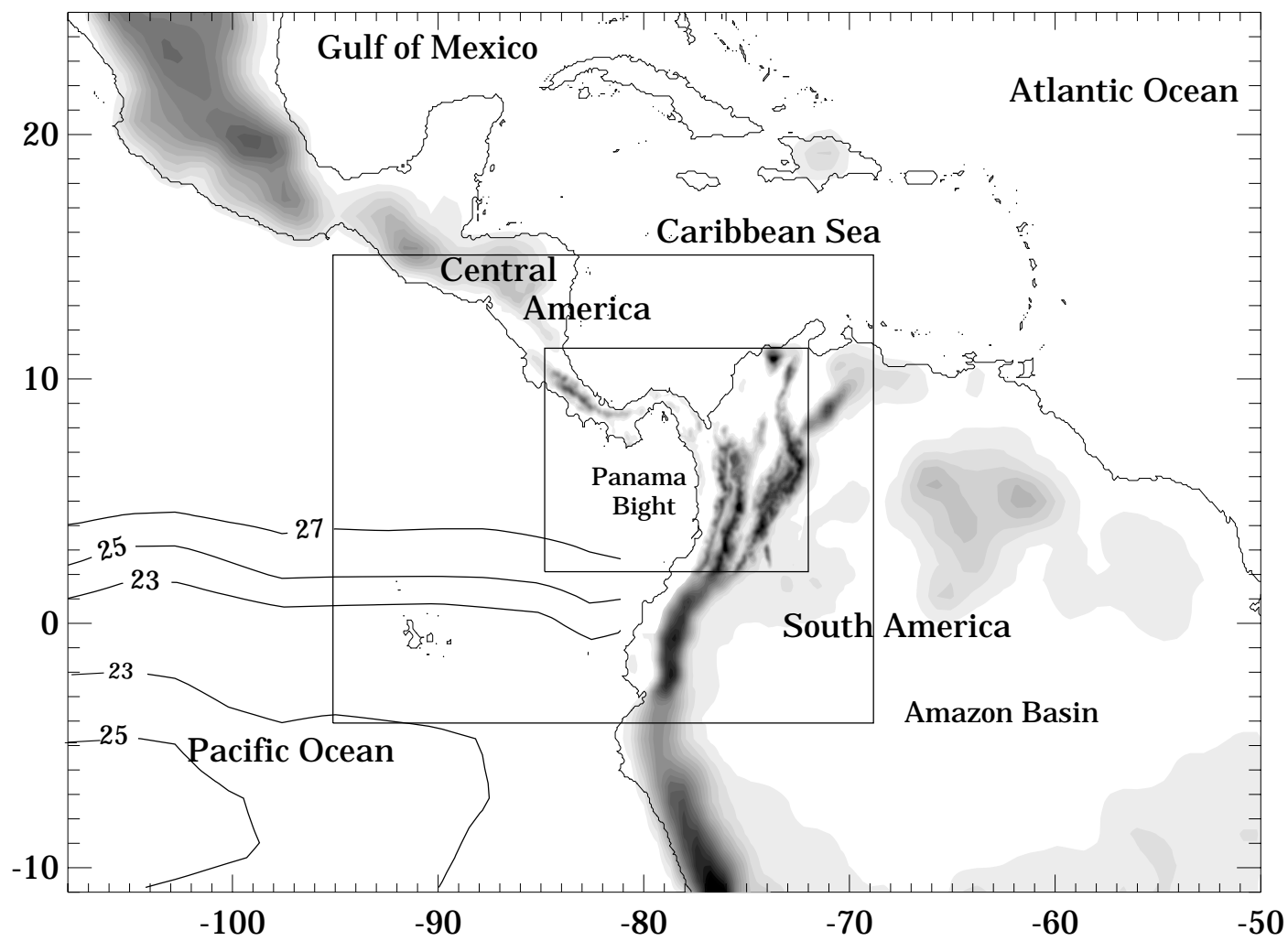
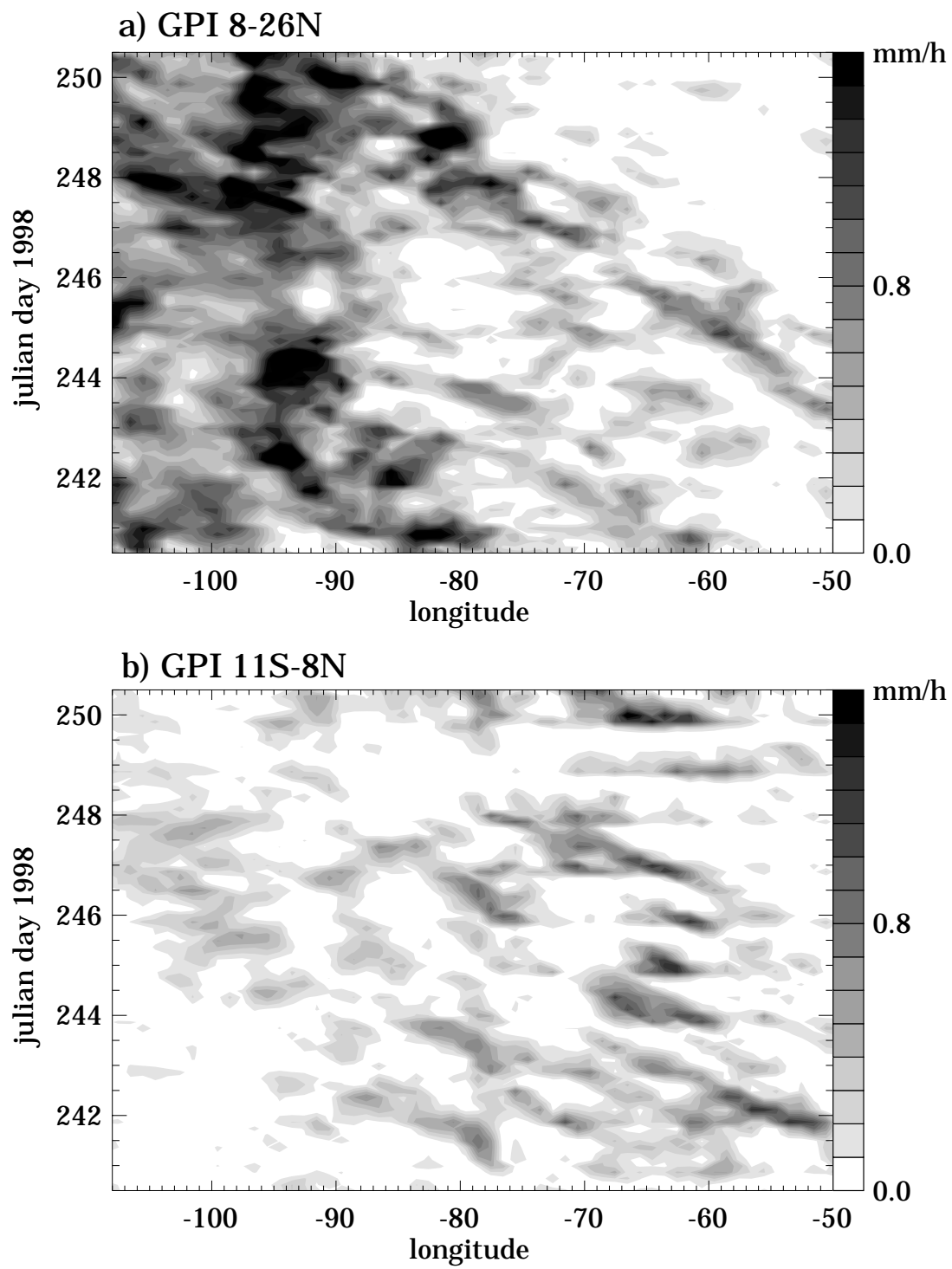


Fig.1

Fig.2



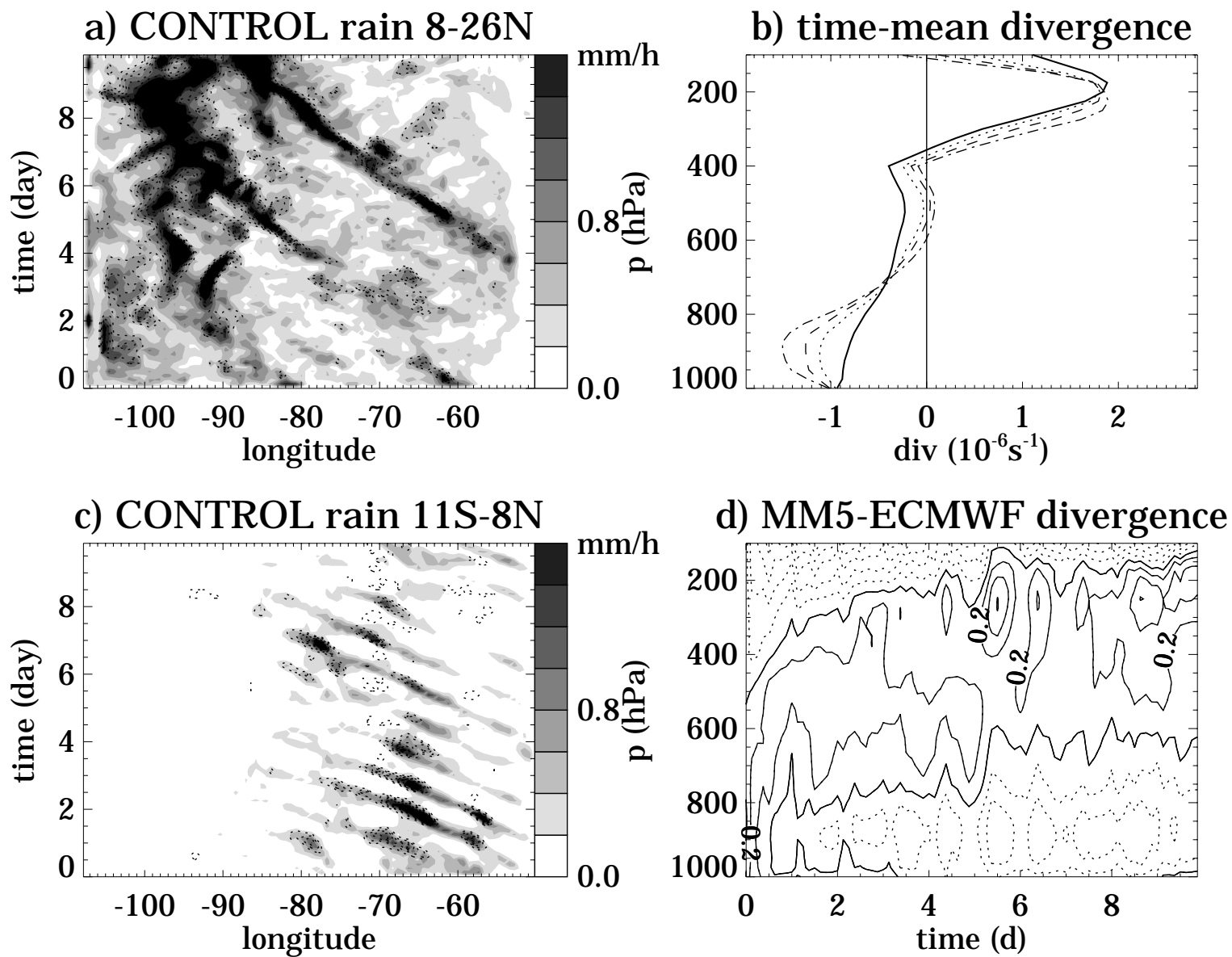


Fig. 3

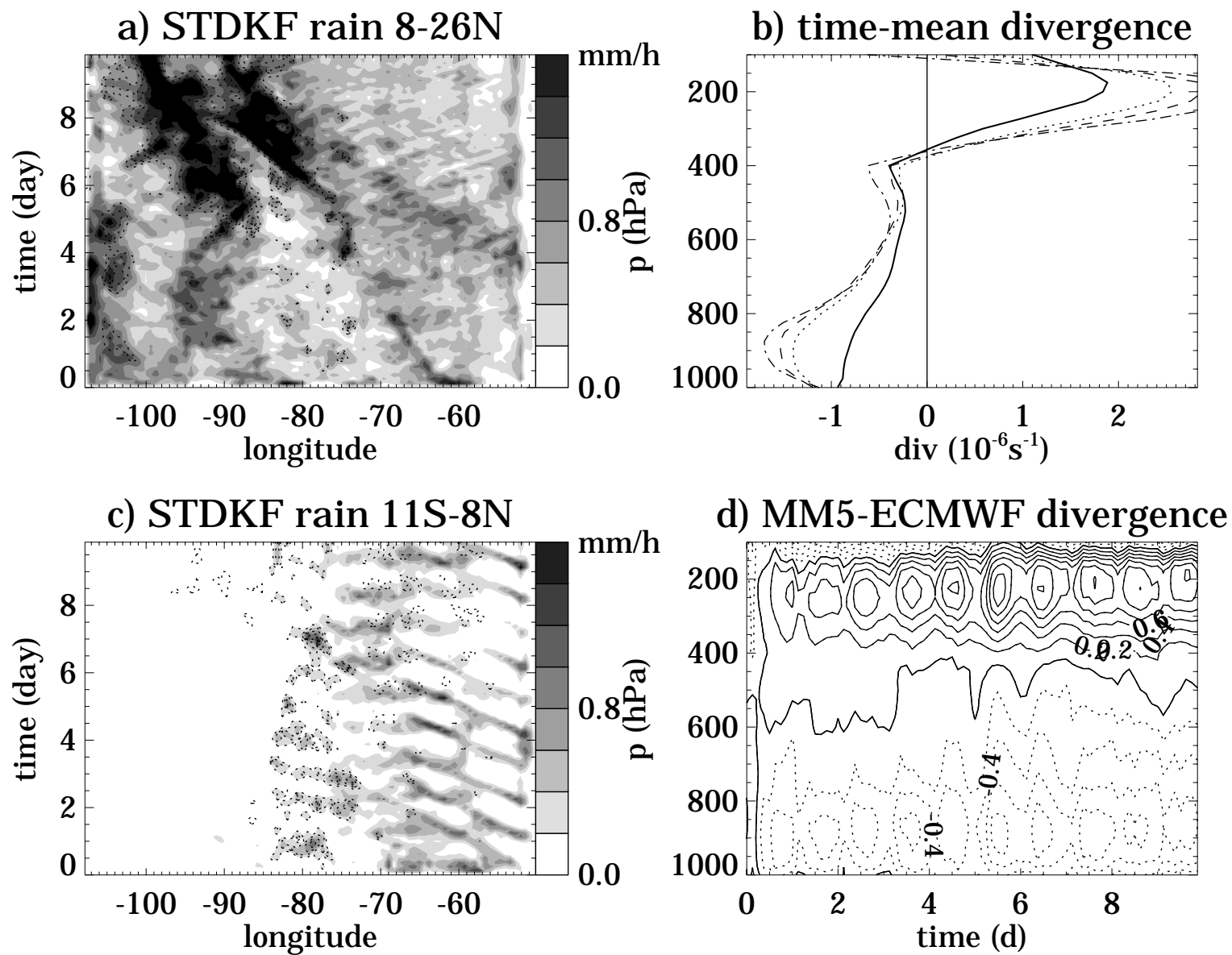


Fig. 4

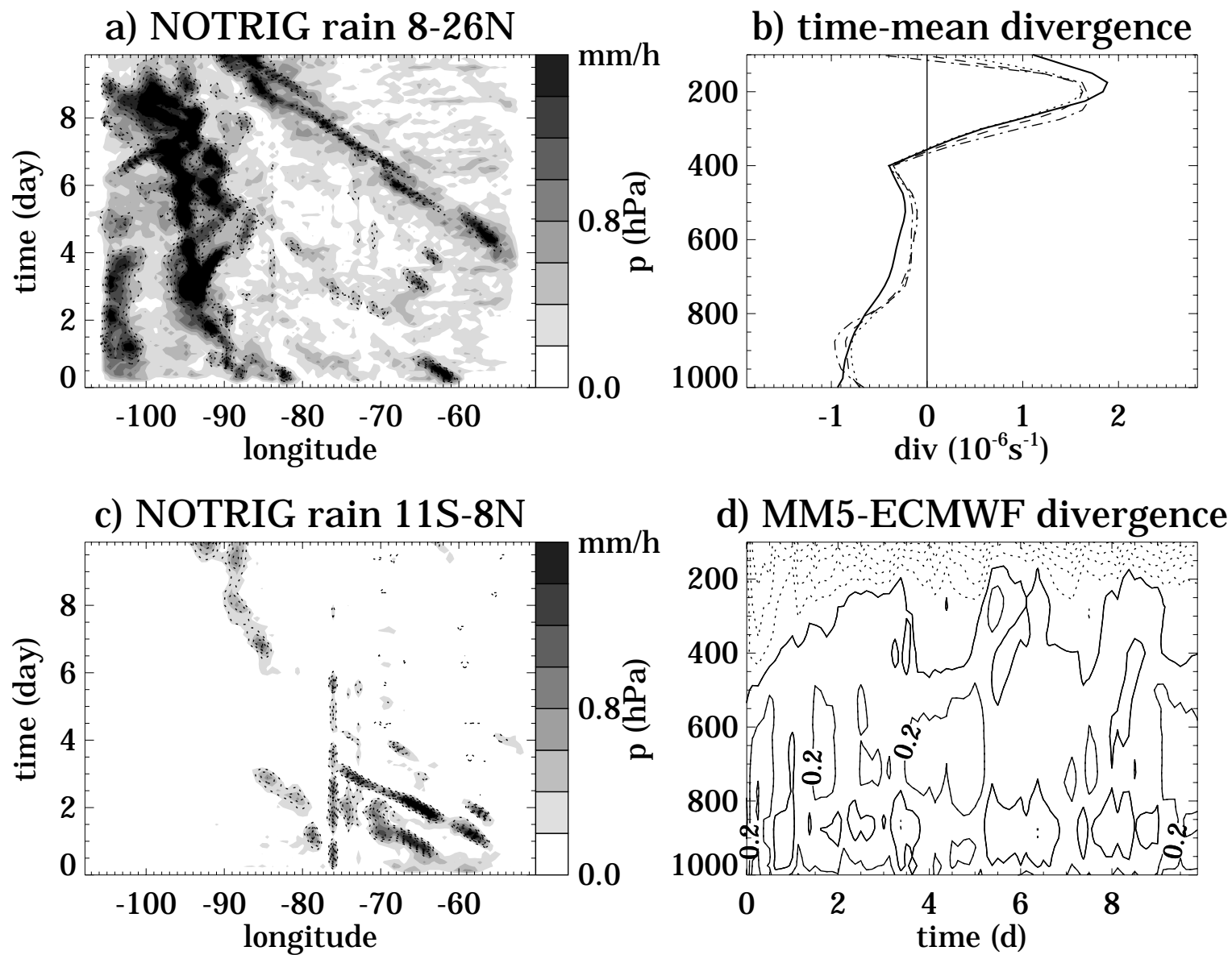


Fig. 5

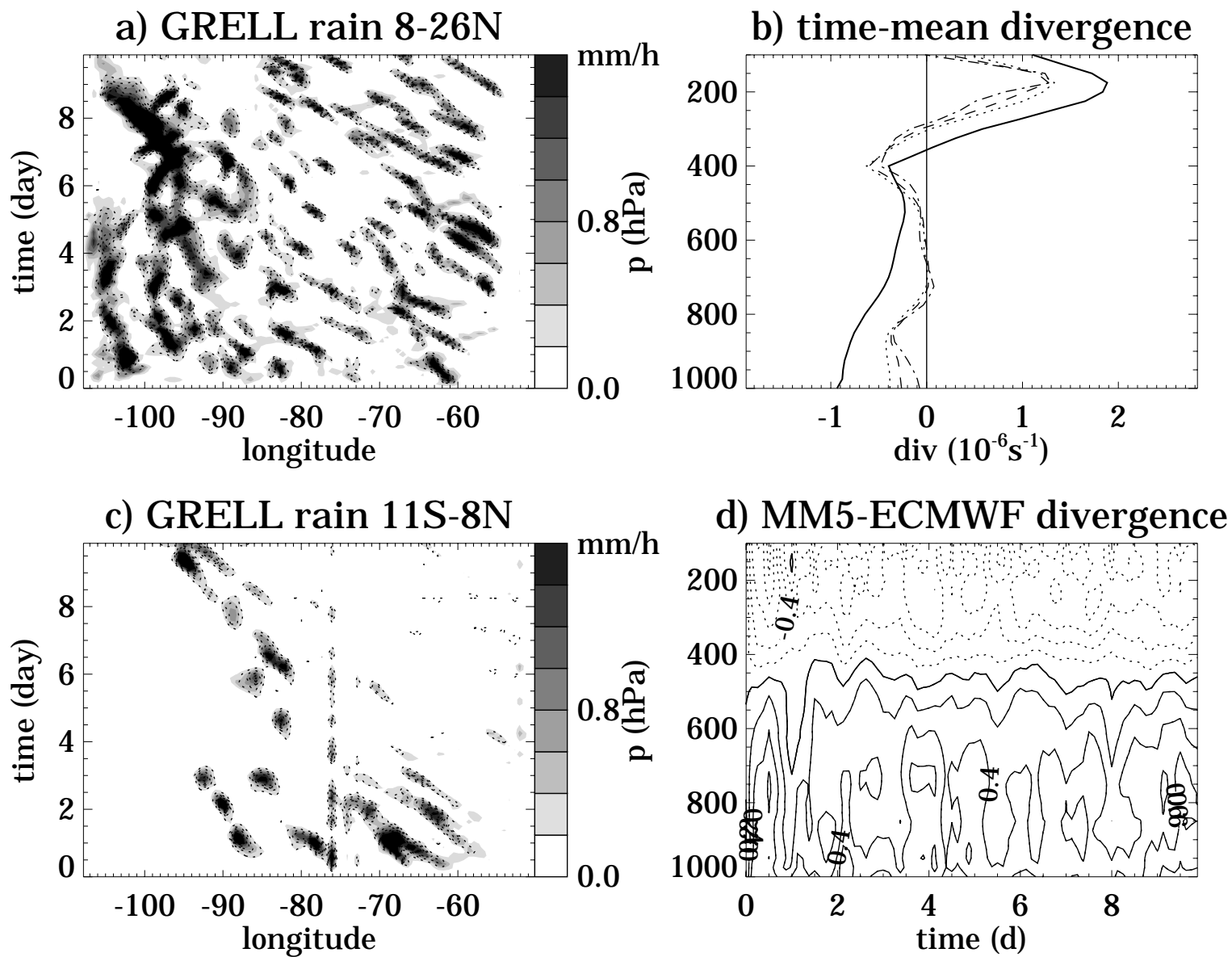


Fig. 6

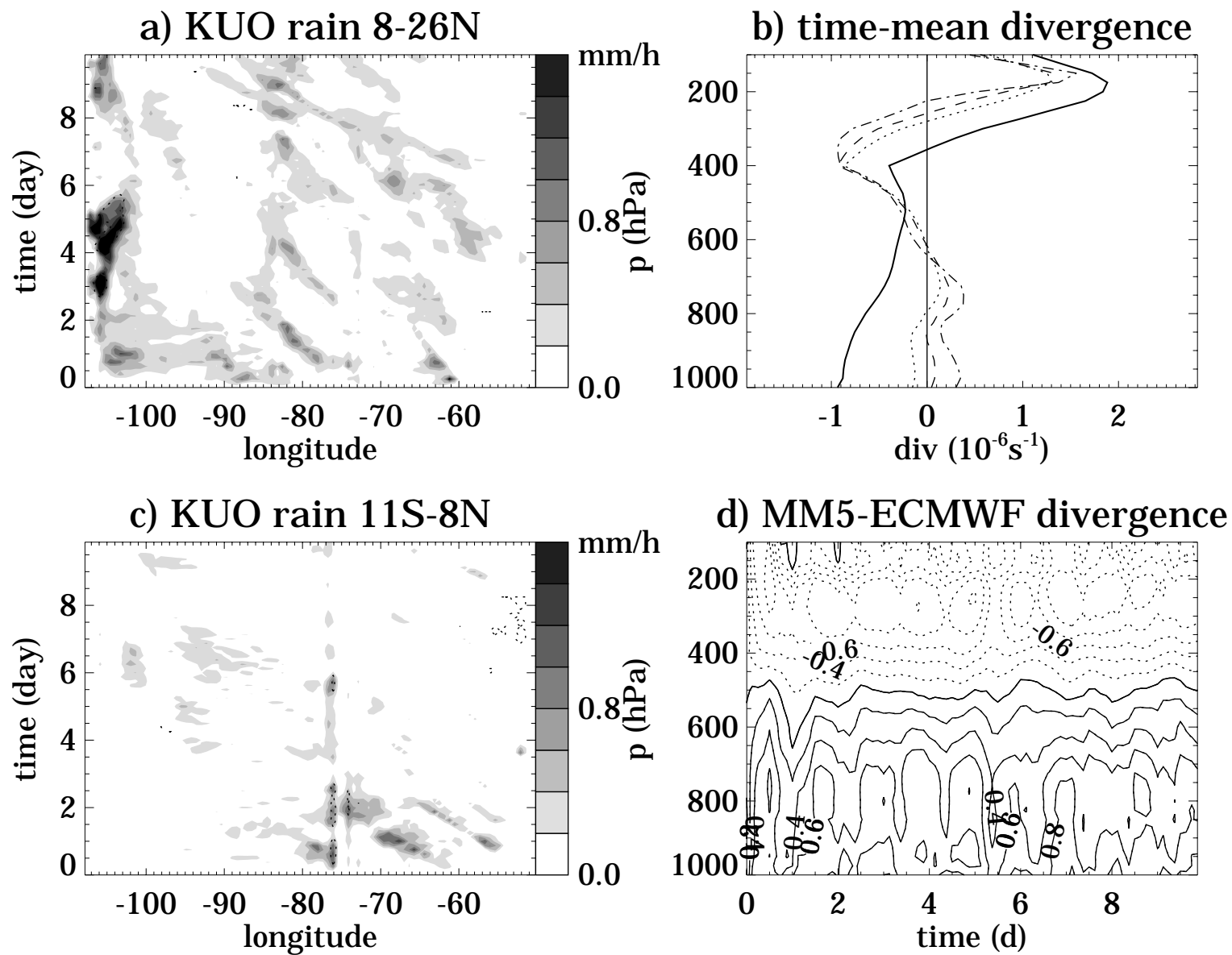


Fig. 7

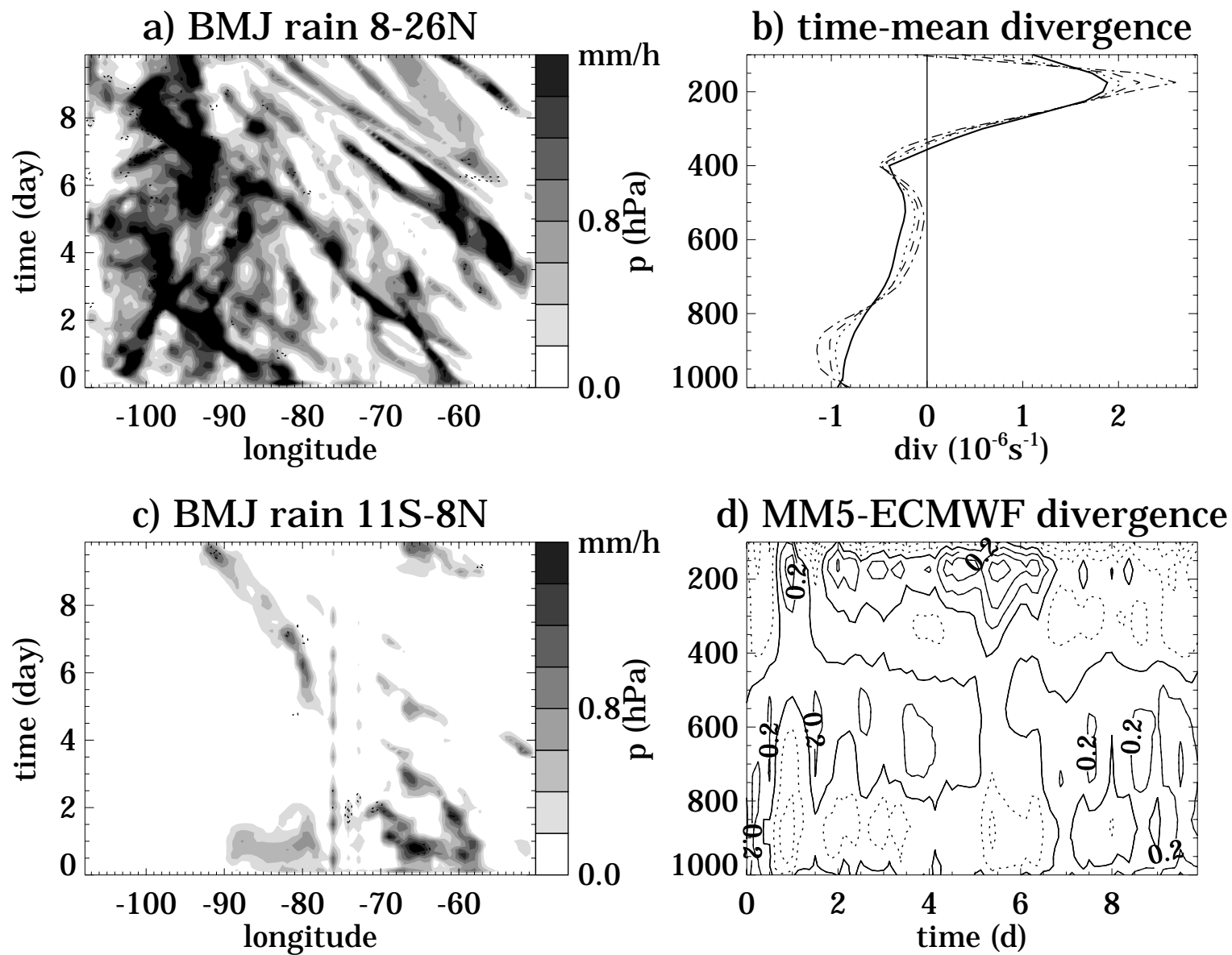


Fig. 8

Fig. 9

